Pressure dependence of spin–orbit levels of Co^{2+} in $KZnF_3$

P. T. C. Freire
Departamento de Fisica, Universidade Federal do Ceará, 60455-760 Fortaleza, CE, Brazil

V. Lemos[a)]
Instituto de Física ''Gleb Wataghin,'' Universidade Estadual de Campinas, UNICAMP, 13083-970 Campinas, São Paulo, Brazil

O. Pilla
Istituto Nazionale di Fisica della Materia, Dipartimento di Fisica, Universitá di Trento, I-38050 Povo, Trento, Italy

N. D. Vieira, Jr.
Instituto de Pesquisas Energéticas e Nucleares, P. O. Box 11 049, 05422-970 São Paulo, SP, Brazil

(Received 21 July 1998; accepted 11 November 1998)

Low temperature emission measurements were performed at atmospheric and high pressures in $KZnF_3:Co^{2+}$. Comparing the zero-phonon line positions and using the phonon dispersion relation of the host material, the fine structure in the emission spectrum was identified. Pressure coefficients were obtained for several among the emission lines from which the values for zero-phonon lines were deduced. Analysis shows that the spin–orbit parameter changes with pressure are negligible in this material. © *1999 American Institute of Physics.* [S0021-9606(99)70608-2]

I. INTRODUCTION

The fluorperovskites doped with transition metal impurities are now of great technological importance as infrared tunable laser materials. Several crystals like $KMgF_3$, MgF_2, $KZnF_3$, or MgO as host to Ni^{2+}, Co^{2+}, and V^{2+} ions can, in principle, be broadly tunable in the wavelength range from 1.5 to 2.4 μm.[1,2] Among those, the Co^{2+}-doped materials are unique because they allow tunability in the infrared, extending far beyond the domain of commercial tunable lasers. In $KZnF_3:Co^{2+}$ a green laser line excites the absorption through the transition $^4T_1(^4F) \rightarrow {}^4T_1(^4P)$. Electrons in the excited state decay nonradiatively to the lowest $^4T_2(^4F)$ level and from there transitions, largely radiative in nature, take place to the ground state $^4T_1(^4F)$ and to the vibronics of these levels. It is those vibronics that are responsible for the broad tunability of these lasers. The electronic transitions involved in the absorption and emission, normally forbidden by inversion symmetry at the site of the substitutional impurity, are made possible only by a perturbation such as spin–orbit coupling, the emission cross section and optical gain being small as a consequence.[3] The question arises as to the possibility to enhance emission, the precursor of laser action, by changing the spin–orbit (SO) parameter, ξ. In principle, a contraction of the lattice should change the electron orbit, thus affecting the Racah parameters and ξ. The analytical calculation of pressure effects on ξ, however, gives conflicting results for ruby, through distinct functions for the relative change of the Racah parameter (B), on pressure (P). One of the approaches dealing on this subject gives a third order power variation of B,[4,5] while others report a square root relation.[6,7] A more recent theoretical treatment by Du *et al.*[8] shows that the change in the SO coupling parameter is smaller than the former results show. The spread of theoretical predictions calls for further investigation, including additional experiments.

We present here a pressure dependence of zero-phonon line emission of $KZnF_3:Co^{2+}$ at low temperatures. The lines were observed to have the same slope within ~9%. This result suggests that the SO coupling parameter does not change appreciably with the pressure.

II. EXPERIMENT

The measurements were performed with a Spex 1870 monochromator and a Ge detector from North Coast Science. Low temperature was achieved by using a closed helium cycle Heli–Tran and 3700 ADP temperature controller (Air Products & Chemicals Inc.), associated with an Au (0.07% Fe)–Chromel thermocouple. The pressure was applied with a gasket diamond anvil cell loaded with Argon as the hydrostatic fluid, as previously described.[9] The luminescence of ruby served to measure the pressure. Single crystals of $KZnF_3:Co^{2+}$ were grown by the Czokralski method with Co incorporation at a concentration of 0.8 mol % (1.2×10^{20} ions/cm^3).

III. RESULTS AND DISCUSSION

The most investigated member of the fluorperovskite-doped family is $KZnF_3:Cr^{3+}$. In this material, however, there is a charge difference between the ion Zn^{2+} and its replacing ion in the octahedral site, Cr^{3+}. Due to this difference, several charge compensation mechanisms required for electrical neutrality lead to different crystal-field sites. The existence of four inequivalent sites for trivalent chromium impurities

[a)]Author to whom correspondence should be addressed. Electronic mail: volia@ifi.unicamp.br

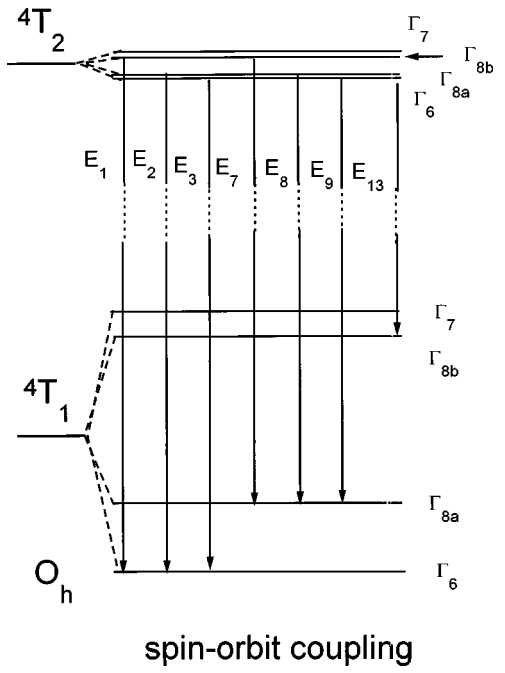

FIG. 1. Energy level diagram for Co^{2+} in $KZnF_3$ illustrating zero-phonon transitions.

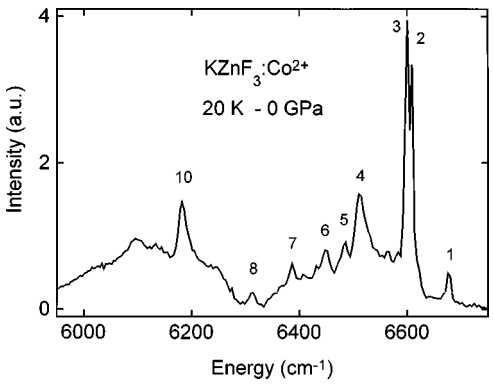

FIG. 2. Emission spectrum of $KZnF_3:Co^{2+}$ taken outside the pressure cell. The mean resolution was about 1 cm^{-1}.

have been reported, three of them observed optically.[10,11] The interpretation of spin-orbit splitting in this material under pressure could be obscured by the increased amount of emission lines originating from each type of site. The task is easier accomplished by selecting a single-site system that requires no charge compensation. Several newly grown divalent transition–metal complexes, like Co^{2+} or Mn^{2+} fluorperovskites,[12] or Ni^{2+} in similar octahedral environments,[13,14] fulfill the single-site symmetry requirement being pure cubic O_h. Although all those materials have spontaneous broadband emission in the infrared, by considering laser action the number of possibilities is reduced. One of the reasons is the presence of strong excited-state absorption in some of these media.[15,16] The others are chemical reasons; Co^{2+}, Mn^{2+}, and Fe^{2+} are the only divalent ions strongly resistant to both oxidation and reduction.[1] Of these, only Co^{2+} has been reported as laser active to date. For those reasons $KZnF_3:Co^{2+}$ was selected in the present investigation. The cobalt electronic configuration ($3d^7$) is described by the free-ion states $^4F,^4P,^4G,^2F,\ldots$, in order of increasing energies. Those states split in the crystal field of the host material. For weak crystal field, the lowest free-ion energy level ^4F is split into $^4T_1,^4T_2$, and $^4A_2$ levels, with $^4T_1$ being the ground state. The main absorptions are due to $^4T_1(^4F) \rightarrow {}^4T_2(^4F), {}^4T_1(^4F) \rightarrow {}^4A_2(^4F)$, and $^4T_1(^4F) \rightarrow {}^4T_1(^4P)$ transitions with characteristic energies of about 7000, 15 000, and 20 000 cm^{-1}, respectively. The emission bands are related to the transition $^4T_2(^4F) \rightarrow {}^4T_1(^4F)$.[17,18] The octahedral crystal field levels are further split by the distortion produced by the spin-orbit interaction into the sublevels that are represented in the diagram of Fig. 1. The spin-orbit splitting is reduced in the $^4T_2$ excited state by the dynamic Jahn–Teller effect, resulting in the quasi-degenerate sublevels (Γ_6,Γ_{8a}) and (Γ_7 and Γ_{8b}), respectively.[19] However, the matrix elements of a $^4T_2 \rightarrow {}^4T_1$ transition being off-diagonal is not affected by the Jahn–Teller effect.[20] The SO coupling, thus, affects the ground state, spreading the $^4T_1$ over some 1000 cm^{-1}. In the diagram of Fig. 1 the sublevels were labeled after Ref. 18 following the same order both in the $^4T_2$ as in the $^4T_1$ terms. The notation $E_i, i=1,2,...$, was adopted here to design the emission energies, the pure electronic transitions being represented in the figure. The transitions are basically magnetic dipole in character. Transitions involving the Γ_7 sublevels, being magnetic dipole forbidden, were not included. The emission spectra of $KZnF_3:Co^{2+}$ recorded at 20 K and atmospheric pressure is shown in Fig. 2. A Pekarian line shape was subtracted from the spectrum in order to emphasize the sharp-line contribution. The line positions in this spectrum are listed in Table I, 3rd column. The strongest lines, marked 2 and 3 in Fig. 2, correspond to the zero-phonon transitions E_2 and E_3 of the diagram in Fig. 1. The lines labeled 7 and 8, were assumed due to the E_7 and E_8 purely electronic transitions as shown in Fig. 1. The remaining lines were interpreted in terms of phonon assisted transitions. The assignments were made by using the following arguments. The zero-phonon lines were identified by direct comparison with the previous results listed in Table I, 5th column. The overall agreement between those results and ours is excellent, the differences in energies being under 5 cm^{-1}.

In order to analyze the phonon assisted transitions, we constructed column 4 of Table I by using the dispersion relation for $KZnF_3$ of Ref. 21 with the following arguments. When the electronic states of the impurity in a crystal are coupled to the vibrations of the lattice, the emission spectrum can be interpreted by using the spectral density of states of the coupled phonon modes. The spectral density of coupled modes results from calculation of the weighted frequencies distribution function by the electron-phonon coupling strength.[22] However, sharp peaks in the phonon density of states occur when the branches of the dispersion curves are flat. At high symmetry points of the Brillouin zone the curves are flat, therefore, it is possible to use the dispersion relation to simplify the analysis of sidebands. Following those arguments, we give in Table II the mean energies taken at high symmetry points in the phonon dispersion curves of $KZnF_3$. The values listed are the experimental points of Ref.

TABLE I. Assignment of sharp-line emission energies and their pressure coefficients. The energies are given in units of (cm^{-1}) and the slopes in (cm^{-1}/GPa).

i	Assignment	E_i 20 K	E_e[a] estimated	E_r[c] 12 K	E_{0i} intercepts	α_i slopes
1	$\Gamma_{8b}(^4T_2)\rightarrow\Gamma_6(^4T_1)$	6673		6675		
2	$\Gamma_{8a}(^4T_2)\rightarrow\Gamma_6(^4T_1)$	6608		6603		
3	$\Gamma_6(^4T_2)\rightarrow\Gamma_6(^4T_1)$	6600		6595	6599	143
4	$E_3-E(X_5)$	6511	6507		6509	139
5	$E_3-E(X_5')$	6483	6475			
6	$E_2-E(X_2')$	6448	6450		6445	128
7	$\Gamma_{8b}(^4T_2)\rightarrow\Gamma_{8a}(^4T_1)$	6387		6382		
8	$\Gamma_{8a}(^4T_2)\rightarrow\Gamma_{8a}(^4T_1)$	6312		6310		
9	$\Gamma_6(^4T_2)\rightarrow\Gamma_{8b}(^4T_1)$		6304[b]	6302		
10	$E_8-E(X_5')$	6183	6187		6183	133
11	$E_8-[E(X_5)+E(X_5')]$		6094		6082	135
12	$E_8-2E(\Gamma_{15})$		6004		~6006	~126
13	$\Gamma_6(^4T_2)\rightarrow\Gamma_{8b}(^4T_1)$			5655	5672	140

[a]Values estimated by subtracting the phonon frequencies from E_i, except for b.
[b]Number obtained by subtraction of the energy separation of levels Γ_{8a} and Γ_6 in the term $^4T_2$ from E_8.
[c]From Ref. 18.

21, or the result of calculation through a rigid ion model (also taken from Ref. 21) in the lack of experimental data. The last column in Table II gives the labeling used for those energies related to the phonon contribution. It should be emphasized that this refers to a distribution of phonons rather than the process involving one phonon of a given symmetry. This procedure is an approximation justified by the fact that the density of states of the coupled phonon modes has maxima corresponding to the frequencies of high symmetry phonons.

It is worth mentioning that additional weak, periodic structures are easily seen in Fig. 2 at the low energy side of peak 3, around peak 7, and around peak 10. The mean energy separation ΔE_j, $j=1,2,3$, are respectively 18.5, 22.1, and 44.2 cm^{-1}. The latter is twice the value ΔE_2. Because some of those weak lines appear on both the high- and low-energy side of a given line with equal separation, we believe them to be phonon sidebands. Optical phonons should not be involved because the energy separations are far below their energy. On the other hand, the branches of the dispersion for acoustic vibrations are spread over several tenths of cm^{-1} for finite wave numbers. Then acoustic phonons should be considered as the origin for those multiple structures observed. However, a closer identification of the phonons is precluded by lack of momentum restriction in this mechanism, in contrast for instance, to the momentum conservation in the zero-wavevector scattering processes occurring with well defined energies.

Next, we discuss the pressure evolution of emission. Spectra taken at four different pressures are shown in Fig. 3. The spectrum marked 0.0 GPa was recorded for the sample outside the pressure cell. It is the unmodified experimental profile taken at $T=20$ K, including the multiphonon contribution. The drastic intensity decay observed on the low energy side of the broadband is caused by the germanium detector cut-off frequency. As the pressure increases the emission spectrum shifts toward higher energies, increasing

TABLE II. Lowest energy values obtained from the phonon dispersion relation of $KZnF_3$ (after Ref. 21). The last column gives the notation employed in Table I.

Branch	Symmetry	ω (cm^{-1})	Notation
acoustics	M_3, R_{25}	77	
acoustic	X_5	93	$E(X_5)$
acoustic	M_3'	119	
acoustic, optics	M_5', X_5'	125	$E(X_5')$
optic	M_2'	137	
optic	R_{15}	147	
optic	Γ_{15}	154	
acoustic	X_2'	159	
optic	Γ_{25}	176	
optic	X_1	183	
optic	X_3	187	
optics	X_5, M_5'	205	

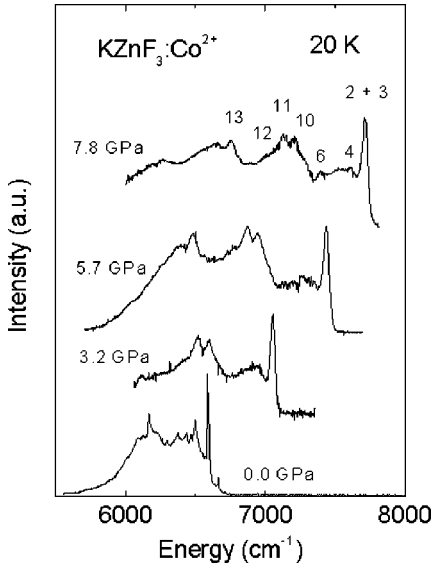

FIG. 3. Emission spectra of $KZnF_3:Co^{2+}$ at several pressure values. The resolution was kept below 3 cm^{-1}.

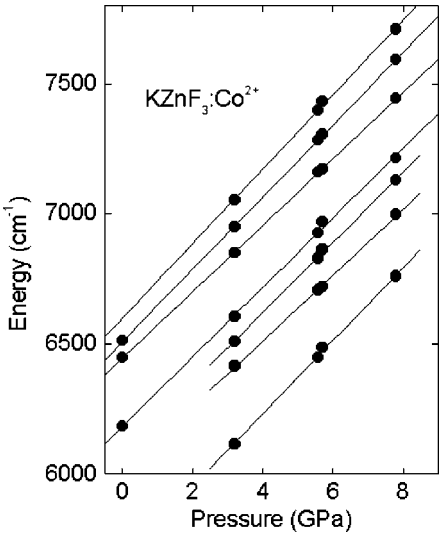

FIG. 4. Pressure dependence of emission energies. The symbols are experimental data and the solid lines are best fit results.

the effective range of detection. As a consequence the spectrum contains additional features at higher pressures. Compare, for instance, the curves labeled 3.2 and 5.7 GPa in Fig. 3. Five lines are clearly observed in the 5.7 GPa spectrum, while only three sharp lines are resolved in the lower pressure spectrum. The highest energy peak in all the $P \neq 0$ spectra corresponds to the overlap of zero-phonon lines 2 and 3, identified in Table I. The next pair of lines at lower energies are assigned as phonon assisted transitions, as described in the table. The upper two curves of Fig. 3 contain another pair of lines but we refer only to one of the lines, marked 13, for which it was possible to determine the pressure dependence of energy, E vs P. The remaining features in the topmost curve were disregarded because of the minor information obtained for those lines. The lack is of no consequence here because the information so far available allows for the general behavior of emission on pressure to be established. The analysis of E vs P for lines 4, 6, and 12 relied on a multiline fitting to Lorentzian line shapes, in order to determine each position. The data were best fitted to straight lines with linear coefficients α_i. The plots E vs P for the main bands described before are given in Fig. 4, where the circles are experimental data and solid lines are the result from the fittings. The resulting pressure coefficients are listed in Table I. Observe in this table that the slopes α_i differ very little among the seven lines analyzed. Due to the negligible pressure shifts of phonons, we consider the phonon-assisted dependence as representative of the corresponding zero-phonon line behavior, to a good approximation. This approach leads to the values $\alpha_2 = 128$ cm^{-1}/GPa and $\alpha_3 = 139$ cm^{-1}/GPa obtained from the analysis of lines 6 and 4, respectively. Comparison of those numbers with the coefficient of the composite line 2+3 indicates a domineering of the E_3 vs P component. The average of α_{10}, α_{11}, and α_{12} was adopted to describe the slope of E_8 vs P, using the same type of argument. The value obtained was $\alpha_8 = 131$ cm^{-1}/GPa. The remaining coefficient, $\alpha_{13} = 140$ cm^{-1}/GPa, was taken directly from the E_{13} vs P plot. Note that the several α_i values thus obtained do not differ appreciably, the differences among them being below 9%. Considering that the spin-orbit parameter ξ is obtained from the Racah parameters and those are deduced from the energy spacings of the levels, as the spacings are kept constant with pressure, so are those parameters. This finding compares favorably with the SO interaction to be unchanged with pressure rather than any of the several functional dependence as proposed before. Notice also in Table I the overall agreement between the intercepts E_{0i} of the curves E_i vs P, and the values E_e estimated as described above. The biggest relative difference does not surpass 0.3%. The agreement being excellent adds further credit to the correctness of the procedure adopted here.

IV. CONCLUSIONS

The emission of $KZnF_3:Co^{2+}$ was studied as a function of pressure at a fixed temperature, $T = 20$ K. The atmospheric pressure results were used to assign several zero-phonon lines by comparison with previous measurements. The phonon-assisted transitions were identified by using the phonon dispersion relation of the host material to estimate the resulting positions. The analysis of the pressure effects allowed for the determination of four zero-phonon line coefficients, α_i, which resulted in the same value within ~9%. This fact yielded the interpretation of a constant SO coupling parameter with pressure for the cobalt levels in fluorperovskite. This result helps clarify a long term dispute on the subject in the past.

ACKNOWLEDGMENTS

We thank the Fundação de Amparo à Pesquisa do Estado de São Paulo (FAPESP), Fundo de Apoio ao Ensino e Pesquisa da Universidade Estadual de Campinas (FAEP/UNICAMP), Fundação Cearense de Amparo à Pesquisa (FUNCAP), and Consiglio Nazionale delle Ricerche (CNR), for financial support.

[1] B. Henderson and G. F. Imbusch, Contemp. Phys. **29**, 235 (1988).
[2] P. F. Moulton, in *Laser Handbook*, edited by M. Bass and M. L. Stitch (North-Holland, Amsterdam, 1985), Vol. 5, pp. 203–288.
[3] N. L. Rowell and D. J. Lockwood, J. Electrochem. Soc. **136**, 3536 (1989), and references therein.
[4] D. P. Ma, X. T. Zheng, Y. S. Xu, and Z. G. Zhang, Phys. Lett. A **115**, 245 (1986); D. P. Ma, X. T. Zheng, Z. G. Zhang, and Y. S. Xu, *ibid.* **121**, 97 (1987).
[5] D. P. Ma, Z. Q. Wang, J. R. Chen, and Z. G. Zhang, J. Phys. C **21**, 3585 (1988).
[6] M. G. Zhao, J. A. Xu, G. R. Bai, and H. S. Xie, Phys. Rev. B **27**, 1516 (1983).
[7] J. A. Xu and M. G. Zhao, Sci. Sin. **24**, 721 (1981).
[8] M. Du, Phys. Lett. A **163**, 326 (1992).
[9] P. T. C. Freire, O. Pilla, and V. Lemos, Phys. Rev. B **49**, 9232 (1994).
[10] M. Mortier, Q. Wang, J. Y. Buzaré, M. Rousseau, and B. Piriou, Phys. Rev. B **56**, 3022 (1997).
[11] O. Pilla, P. T. C. Freire, and V. Lemos, Phys. Rev. B **52**, 177 (1995).
[12] M. C. M. de Lucas, F. Rodrigues, and M. Moreno, Phys. Rev. B **50**, 2760 (1994), and references cited therein.
[13] E. Martins, M. Duarte, S. L. Baldochi, S. P. Morato, M. M. F. Vieira, and N. D. Vieira, Jr., J. Phys. Chem. Solids **58**, 655 (1997).
[14] R. J. Sherlock, T. J. Glynn, G. Walker, G. F. Imbusch, and K. W. Godfrey, J. Lumin. **72**, 268 (1997).

[15] N. V. Kulesshov, V. G. Shcherbitsky, V. P. Mikhailov, S. Kuck, J. Koetke, K. Petermann, and G. Huber, J. Lumin. **71**, 265 (1997).
[16] A. J. Wojtowiccz, Acta Phys. Pol. A **80**, 193 (1991).
[17] W. Künzel, W. Knierim, and U. Dürr, Opt. Commun. **36**, 383 (1981).
[18] H. Manaa, Y. Guyot, and R. Moncorge, Phys. Rev. B **48**, 3633 (1993).
[19] M. D. Sturge, Phys. Rev. B **8**, 6 (1973).
[20] M. D. Sturge, Phys. Rev. B **1**, 1005 (1970).
[21] M. Rousseau, J. Y. Gesland, B. Hennion, G. Heger, and B. Renker, Solid State Commun. **38**, 45 (1981); see also: N. Lehner, H. Rauh, K. Strobel, R. Geick, G. Heger, J. Bouillot, B. Renker, M. Rousseau, and W. G. Stirling, J. Phys. C **15**, 6545 (1982).
[22] U. Dürr and R. Weber, Solid State Commun. **14**, 907 (1974).